Assessment of Stability and Control Interaction Risks in PV Parks with Two-Stage Grid-Forming Control

Dabeaurard Tho
Department of Electrical Engineering
Polytechnique Montreal
Montreal, Canada
dabeaurard.tho@polymtl.ca

Jean Mahseredjian
Department of Electrical Engineering
Polytechnique Montreal
Montreal, Canada
jean.mahseredjian@polymtl.ca

Antoine Lesage-Landry
Department of Electrical Engineering
Polytechnique Montreal
Montreal, Canada
antoine.lesage-landry@polymtl.ca

Nasim Rashidirad
Department of Simulation of Networks
Hydro-Québec Research Institute
Varennes, Canada
rashidirad.nasim@hydroquebec.com

Alireza Masoom
Department of Simulation of Networks
Hydro-Québec Research Institute
Varennes, Canada
masoom.alireza@hydroquebec.com

***Abstract*— The stability of grid-forming (GFM) inverter-based resources (IBRs) is typically analyzed under the assumption that they are supplied by batteries or ideal DC sources, without accounting for variations in the DC link voltage. This paper contributes to small-signal stability analysis of photovoltaic (PV) parks operating in a two-stage GFM configuration: reserve grid-forming mode (R-GFM), which provides power reserves, and limited grid-forming mode (L-GFM), which delivers the maximum available power. A transition strategy between these modes is adopted and validated. Numerical simulations are conducted in EMTP® on a PV park connected to a weak grid under both standard and low irradiance conditions, comparing the two-stage GFM operation to the standard grid-following (GFL) control. Results show that the PV park preserves system stability in GFM modes, whereas instability occurs under GFL operation.**

Keywords— Grid-following, grid-forming, impedance-based stability assessment, photovoltaic.

I. Introduction

Power systems are undergoing significant transformation as an increasing share of generation comes from inverter-based resources (IBRs), e.g., solar and wind. This transition reduces the presence of conventional synchronous machines, which traditionally provide inertia. Consequently, modern grids have become more sensitive to disturbances. While IBRs typically operate in grid-following (GFL) mode to synchronize with and support grid power and frequency, grid-forming (GFM) IBRs offer a promising alternative, particularly in microgrids and autonomous systems where both control schemes coexist [1].

Various strategies have been developed for GFM control, including droop, virtual synchronous machine, matching, and virtual oscillator control, each offering distinct advantages and trade-offs [2]. Comparative stability analyses of these approaches have been widely discussed in the literature [2]. However, most studies assume that the inverter is connected to an ideal DC source [2][3]. While such assumption simplifies the analysis, it neglects the dynamics of real energy sources, e.g., irradiance variations. Renewable energy sources are inherently non-dispatchable, meaning their power output depends on environmental conditions. This introduces challenges for maintaining system stability and providing ancillary services. To address these challenges, two main solutions have been proposed: (1) Energy storage or load shedding when the PV park operates below its maximum power point (MPP) [4]; (2) Two-stage GFM control [4], comprising reserve GFM mode (R-GFM) and limited GFM mode (L-GFM). In the R-GFM mode, the inverter maintains a power reserve, enabling fast frequency response and inertia-like behavior. Conversely, in the L-GFM mode, the PV park operates at its MPP, leaving no reserve for voltage or frequency regulation.

A. Research Motivation

Despite the growing interest in GFM control, the stability of PV parks operating under realistic conditions, such as fluctuating irradiance and DC link voltage variations remains insufficiently explored. Existing studies largely neglect these dynamics, limiting their applicability to real-world scenarios. This gap is critical because weak grids and microgrids with high PV penetration are increasingly common, and their reliable operation depends on robust stability under varying conditions.

B. Contribution

This paper addresses the small-signal stability analysis of a PV park operating in a new two-stage GFM configuration. A transition strategy between the R-GFM and L-GFM modes is implemented in EMTP® [5]. The functionality of the architecture is compared to a PV park connected to a weak grid and operating in GFL mode under two different irradiance conditions. Time-domain simulations and impedance-based stability assessment (IBSA) methods are employed to validate the system's performance.

The rest of this paper is organized as follows: Section II introduces the two-stage GFM approach and details its implementation in EMTP®. Section III presents the simulation results and discusses their implications. Section IV concludes the paper and outlines potential directions for future work.

II. Two-stage GFM Control Scheme

The two-stage GFM control scheme builds upon the generic method presented in [6]. To achieve this, a DC–DC converter is

979-8-3315-8138-1

integrated into the original PV park converter controller to regulate the DC-link voltage in both R-GFM and L-GFM modes [4]. Fig. 1 illustrates the implementation of the power components and controller of PV parks in EMTP®. Additionally, a transition mechanism is incorporated to enable smooth switching between R-GFM and L-GFM modes under varying operating conditions.

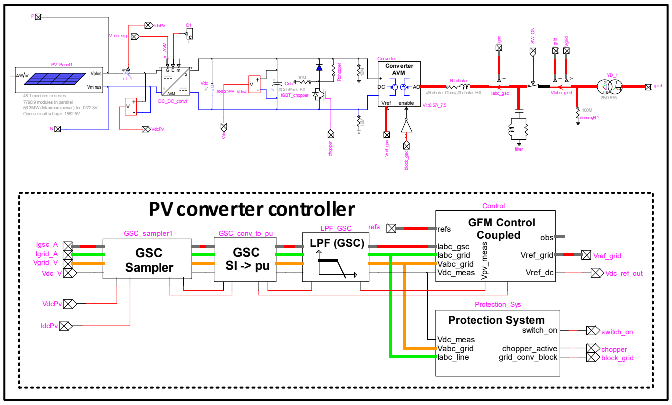

Fig. 1. PV park and PV converter controller designed in EMTP®.

A. Droop Control Structure

The original droop control equation is expressed as:

$$\omega = \omega_0 + k_f \left(P_{ref} - P_{act}\right) \quad (1)$$

$$v = v_{ref} + k_v (Q_{ref} - Q_{act}) \quad (2)$$

where ω and ω_0 denote actual and nominal angular frequency (rad/s), P_{ref} is the reference active power, P_{act} is the measured active power, v and v_{ref} are the voltage sent to the inner controller and nominal reference voltage, Q and Q_{ref} denotes the measured and reference reactive power, and k_f and k_v are droop coefficients for frequency-power and voltage-reactive power sensitivity.

In the R-GFM mode, the frequency follows the same droop characteristics as a synchronous machine, allowing the converter to emulate its inertia and frequency response. However, in L-GFM, an additional frequency correction term $\Delta\omega$ is introduced in the droop equation. The correction term is derived from the deviation between the measured DC-link voltage v_{dc} and its reference v_{dc}^{ref} through a PI controller [4]. The correction mechanism is activated only when the system operates in L-GFM mode; otherwise, the inverter adheres to the original droop control equation.

$$\omega = \omega_0 + d_f \left(P_{ref} - P_{act}\right) + \left(k_p + k_i \frac{1}{s}\right)\left(v_{dc} - v_{dc}^{ref}\right) \quad (3)$$

where k_p and k_i are the coefficients of PI controller.

B. DC-DC Converter and Controller Structure

The PV arrays in the park are interfaced with the DC-link through a boost DC–DC converter. Fig. 2 illustrates the control scheme architecture. Fig. 3 illustrates P–V characteristics of the two-stage PV system operating under different grid-forming modes.

In the R-GFM mode, the DC–DC converter regulates the DC-link voltage to balance power flow between the PV array and the inverter. Unlike conventional MPP operation, the PV array is intentionally operated above its MPP voltage, reducing the extracted power and creating a power reserve. This reserve allows the inverter to increase or decrease its active power output in response to grid frequency deviations, emulating the inertial and frequency response of synchronous machines.

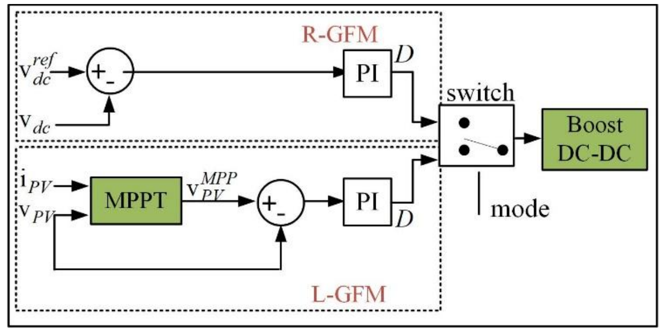

Fig. 2. The schematic of the DC-DC controller of PV park.

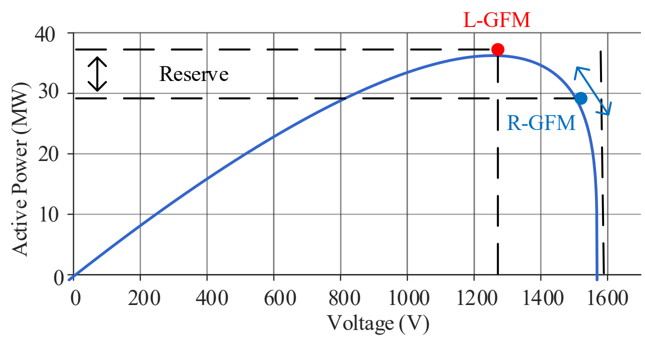

Fig. 3. P–V characteristics of the two-stage PV system operating under different grid-forming modes.

In the L-GFM mode, the MPPT algorithm continuously calculates the optimal PV voltage, v_{MPP} that corresponds to the maximum power point under current irradiance and temperature conditions. This value serves as the reference voltage for the PV array in the L-GFM mode. The PI controller compares the reference PV voltage from the MPPT algorithm, v_{ref}^{MPP} to the measured PV voltage, v_{PV}. The error signal is processed by the PI controller to generate the duty cycle D for the boost DC–DC converter:

$$D = (k_{pD} + k_{iD} \frac{1}{s})\left(v_{ref}^{MPP} - v_{PV}\right) \quad (4)$$

where k_{pD} and k_{iD} are the coefficients of PI controller.

C. Mode Transition Strategy

The transition between the R-GFM and L-GFM modes is governed by the DC-link voltage and system frequency deviation. Fig. 4 illustrates the flowchart of this process. Under normal operating conditions, the PV park functions in the R-GFM mode, maintaining a power reserve for grid support.

979-8-3315-8138-1

When a significant disturbance occurs, the inverter demands more power than the PV array can supply, causing the DC-link voltage to drop. If the voltage falls below a predefined threshold v_{dc}^{min}, the controller switches to the L-GFM mode. In this mode, the DC–DC boost converter activates MPPT control to extract the maximum available PV power. Once the operating point returns within the PV capacity and the frequency deviation is eliminated, the system transitions smoothly back to the R-GFM mode.

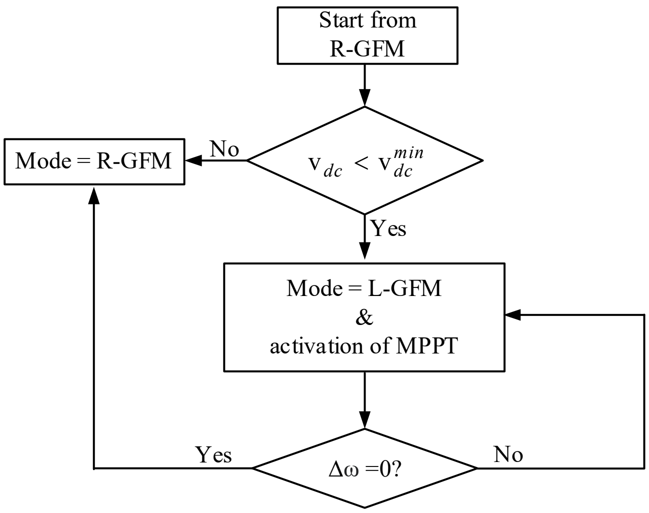

Fig. 4. Mode transition strategy flowchart.

III. Simulations And Results

Fig. 5 illustrates the test circuit developed to evaluate the two-stage GFM control scheme and its impact on system stability. The system consists of two PV park connected to an ideal voltage source through two parallel transmission lines, each 50 km in length, modeled using constant-parameter representation. Only one is active during each simulation. The ideal voltage source is equipped with a series RL impedance to emulate the Thevenin equivalent of the grid. Each PV park has a rated capacity of 75 MVA under standard test conditions (irradiance of 1000 W/m² and temperature of 25 °C). PV_Park1 can operate in L-GFM or R-GFM, whereas PV_Park2 operates in GFL mode [7]. The grid strength is characterized by a short-circuit ratio (SCR) of 2.5, indicating a weak grid scenario.

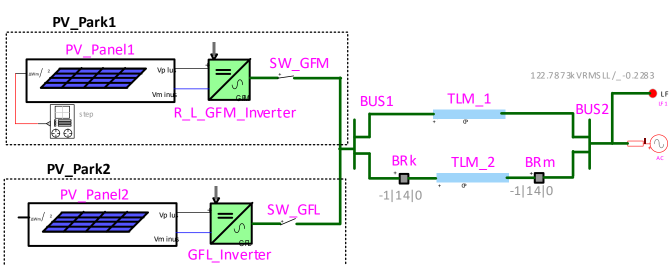

Fig. 5. Test case circuit includes the PV_Park1 working in either L-GFM or R-GFM mode, and PV_Park2 working in GFL mode.

A. Dynamic Behavior of the GFM Inverter

This case study evaluates the mode transition capability of PV_Park1 under varying irradiance conditions. At time $t = 4$ s the irradiance begins to decrease from 1000 W/m² to 750 W/m² at $t = 5$ s. It then remains constant until $t = 20$ s. Afterward, it ramps back to its initial value over 1 s. The irradiance profile is shown in Fig. 6.(a).

The simulation starts in R-GFM mode. Initially, the PV park delivers 60 MW (Fig. 6.(b)). As irradiance decreases, the available power drops to approximately 44 MW. During this reduction, the output power remains constant because the available power exceeds the reference setpoint. However, the DC-link voltage exhibits a gradual decline, as the MPP voltage decreases with irradiance. When the DC-link voltage reaches its threshold (e.g., $v_{dc}^{min} = 0.95 v_{dc}$), a mode transition occurs, and the L-GFM mode is activated. At this point, the frequency correction term becomes active, restoring the DC-link voltage to its nominal value (Fig. 6.(c)). When irradiance ramps back to 1000 W/m², the available power increases, causing the frequency deviation to gradually return to zero (Fig. 6. (d)). This enables a smooth transition back to the R-GFM mode. Thereafter, the power output stabilizes at its reference value of 60 MW (Fig. 6. (b)).

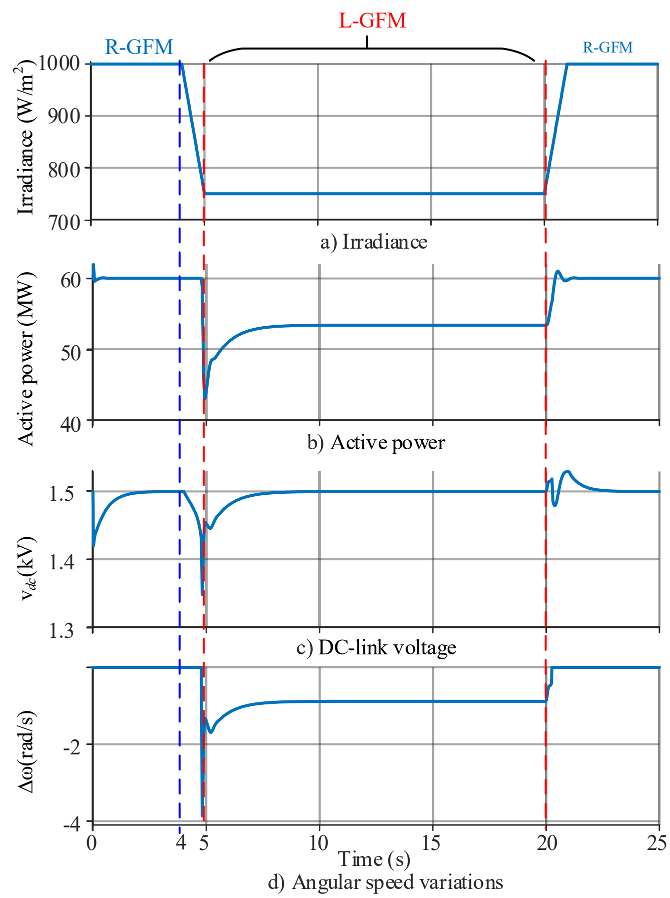

Fig. 6. Simulation results of PV_Park1 and its transition between R-GFM and L-GFM modes

B. Stability Comparison Between GFM and GFL Modes

In this test, the irradiance is initially set to 500 W/m² to represent a low-generation condition. Grid stability is then compared in GFM and GFL modes. A disturbance is introduced by disconnecting transmission line TLM_2 in Fig. 5 at $t = 14$ s,

979-8-3315-8138-1

further reducing grid strength. The simulation runs for 20 s with a time step of 25 µs in EMTP®.

Fig. 7 compares the PV system's output current and power for three modes: L-GFM (blue) and R-GFM (red) using PV_Park1, and GFL using PV_Park2 GFL (green). The results indicate that the PV park operating under the two-stage GFM scheme remains stable in both L-GFM and R-GFM modes following the disturbance. In contrast, when operating in GFL mode, oscillations of approximately 40 Hz appear in the output power. Similar oscillations are observed in the output current, confirming the reduced stability margin in GFL mode. Fig. 8 presents the fast Fourier transform (FFT) analysis of the PV park current, revealing two additional frequency components around 20 Hz and 100 Hz besides the fundamental frequency. The super-synchronous component near 100 Hz exhibits a higher magnitude than the sub-synchronous component at 20 Hz, indicating a control interaction instability at high frequency. The sub-synchronous component is attributed to the mirror frequency phenomenon [8].

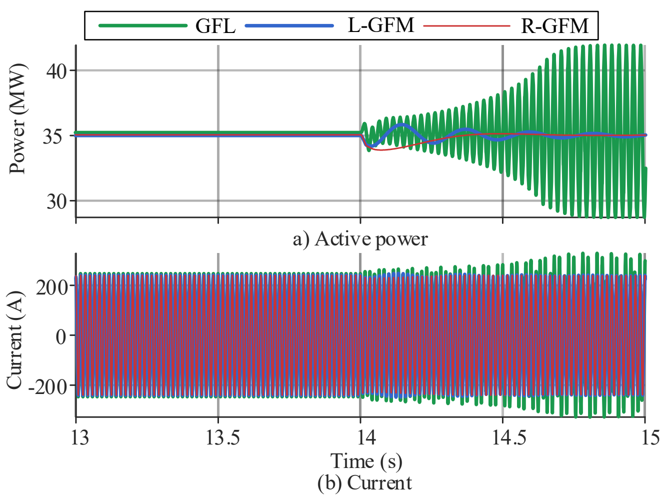

Fig. 7. PV park output at Bus 1 for three operating modes

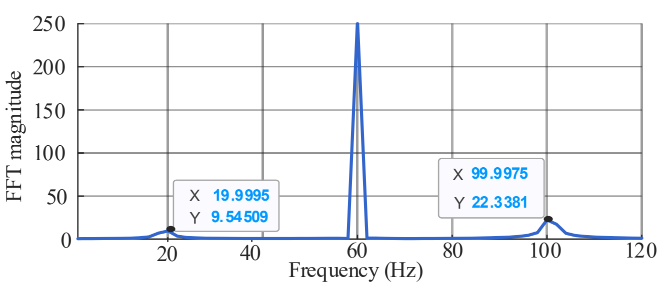

Fig. 8. Frequency spectrum of the output current of PV_Park2.

C. *Stability Assessment Using IBSA Method*

The stability of different inverter configurations can be evaluated in the frequency domain [9]. IBSA provides a systematic approach to characterize inverter-grid interactions across a wide frequency range, identifying potential resonances and passivity violations. The first comparison is performed between GFL and L-GFM modes. Fig. 9 illustrates the positive sequence impedance scans for both systems. In the GFL case (Fig. 9.(a)), the resistance exhibits negative values at low frequencies, indicating potential instability. Contrastingly, the L-GFM case (Fig. 9.(b)) maintains positive resistance over most of the frequency range, with only a small negative resistance region near the fundamental frequency. The L-GFM controller demonstrates a broader region of positive resistance compared to GFL, highlighting its ability to enhance small-signal stability by mitigating negative resistance effects. It is also important to note that impedance magnitudes in GFL and L-GFM modes differ significantly, which is typically assumed in stability analysis.

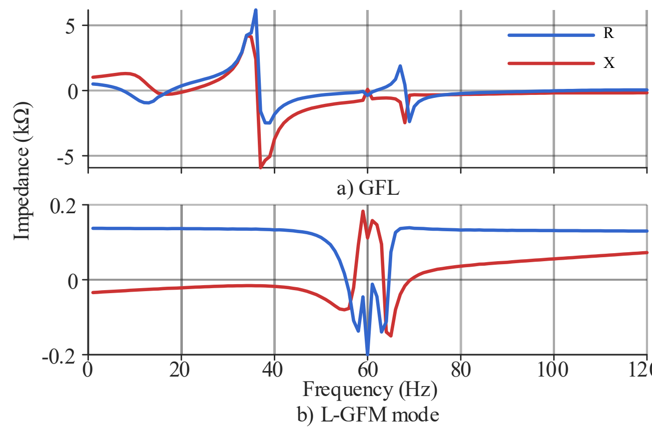

Fig. 9. Comparison of positive-sequence impedance of PV park

System stability can be evaluated using the reactance crossover criterion (RCC), applied to the positive sequence impedance obtained from frequency scanning [9]. The criterion of instability is given by:

$$R_{\Sigma}(f)\left.\frac{dX_{\Sigma}(f)}{df}\right|_{f=f_c} < 0 \tag{5}$$

where R_{Σ} is the combined resistance, representing the sum of the resistances of the IBR and the grid, X_{Σ} is the combined reactance, corresponding to the sum of the reactances of the IBR and the grid, and f_c is the frequency at which the combined reactance crosses zero. Fig. 10 shows the positive sequence combined impedance of the PV park and the grid in GFL mode. Notice that the combined reactance crosses zero three times, at 14.3 Hz, 21 Hz, and 100 Hz. The instability occurs at around 100 Hz when applying the RCC, which is consistent with the FFT results presented in Fig. 8.

Fig. 11 illustrates the positive-sequence combined impedance of the PV park and the grid in L-GFM mode. One can see that the combined reactance also crosses zero three times, at 14 Hz, 64 Hz, and 65.5 Hz. For these three frequencies, the system satisfies the RCC condition and remains stable. Fig. 12 compares the impedances of the PV park in R-GFM and L-GFM modes. One can see that both modes exhibit similar impedance profiles. Beyond the fundamental frequency, the impedance responses are nearly identical, implying similar small-signal stability margins. Near the fundamental frequency, the differences indicate that the L-GFM mode is more prone to instability. The resistance decreases close to the fundamental frequency in both cases; however, the L-GFM mode exhibits a more significant negative resistance region. Moreover, the

979-8-3315-8138-1

reactance of the L-GFM mode shows additional zero-crossings near the fundamental frequency, with three crossings compared to only one in the R-GFM mode. According to the RCC, this behavior increases the risk of resonance interactions when connected to the grid, particularly under strong grid conditions where the grid reactance is relatively low.

In this example, the PV park operating in the GFM mode exhibits superior stability performance. However, when operating in the L-GFM mode, the system becomes more prone to instability than in the R-GFM mode.

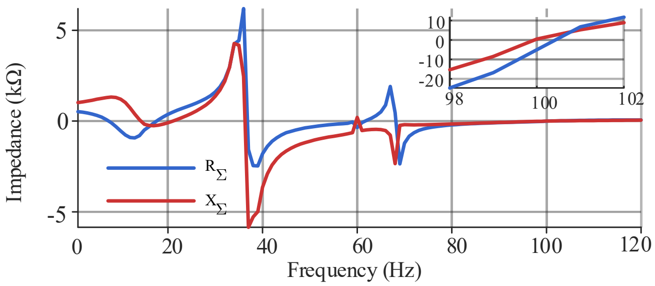

Fig. 10. Positive sequence combined impedance scan of grid and PV park in GFL mode.

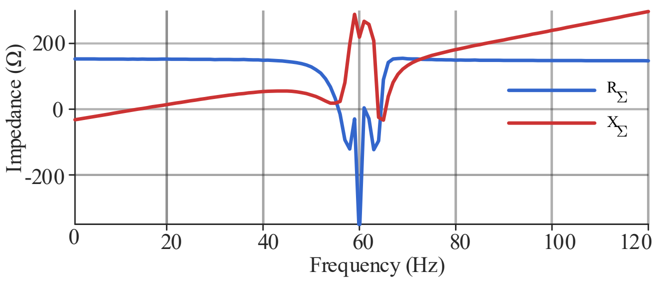

Fig. 11. Positive sequence combined impedance scan of grid and PV park in L-GFM mode.

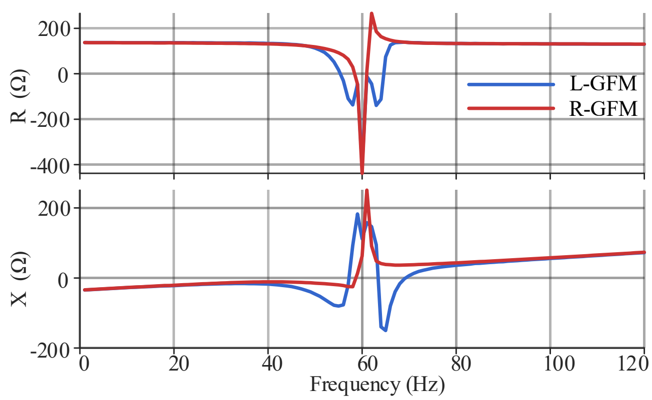

Fig. 12. Comparison of the PV impedance scan between L-GFM and R-GFM modes

IV. Conclusion

This paper investigated the stability of PV parks operating under two-stage GFM and single-stage GFL modes using time-domain simulations and impedance-based stability analysis. Numerical simulations illustrates that the GFL controller exhibits negative resistance at low frequencies and becomes unstable under weak grid conditions, whereas the two-stage GFM controller maintains positive resistance.

Among GFM configurations, the overall impedance behavior is similar; however, near the fundamental frequency, the L-GFM mode shows a stronger negative resistance component and additional reactance zero-crossings, indicating a higher risk of small-signal instability compared to the R-GFM mode. The study confirms that the two-stage GFM approach can significantly enhance system stability, even when operating below the maximum power point, by leveraging control strategies rather than costly battery storage solutions. This enables grid-forming functionality while improving stability under weak grid conditions.

Future work will focus on extending this concept to larger multi-IBR networks and quantitatively evaluating the trade-off between power reserve allocation and energy production under realistic PV and grid operating conditions.

References

[1] R. Rosso, X. Wang, M. Liserre, X. Lu, and S. Engelken, "Grid-Forming Converters: Control Approaches, Grid-Synchronization, and Future Trends—A Review," IEEE Open J. Ind. Applicat., vol. 2, pp. 93–109, 2021.

[2] J. Peralta, V. Velar, E. Quintana, J. Mahseredjian, H. Gras, and H. Ashourian, "Dynamic Behavior of Grid-forming Inverters in Large-scale Low-strength Power Grids," in 2024 IEEE/PES Transmission and Distribution Conference and Exposition (T&D), Anaheim, CA, USA: IEEE, May 2024, pp. 1–5.

[3] H. Zhang, W. Xiang, W. Lin, and J. Wen, "Grid Forming Converters in Renewable Energy Sources Dominated Power Grid: Control Strategy, Stability, Application, and Challenges," Journal of Modern Power Systems and Clean Energy, vol. 9, no. 6, pp. 1239–1256, 2021.

[4] B. Pawar, E. Batzelis, S. Chakrabarti, and B. Pal, "Grid-Forming Control for Solar PV Systems with Power Reserves," *IEEE Trans. Sustain. Energy*, vol. 12, no. 4, pp. 1947–1959, Oct. 2021.

[5] J. Mahseredjian, S. Dennetière, L. Dubé, B. Khodabakhchian, and L. Gérin-Lajoie, "On a new approach for the simulation of transients in power systems," Electric Power Systems Research, vol. 77, no. 11, pp. 1514–1520, Sept. 2007.

[6] Hossein Ashourian, and Henry Gras, "Three-phase Grid Forming Inverter." EMTP, 2022, [online available in]: www.emtp.com

[7] U. Karaagac, H. Ashourian, I. Kocar, A. Stepanov, H. Gras, and and J. Mahseredjian, "PV Park Models in EMTP." EMTP, 2022, [online available in]: www.emtp.com

[8] A. Masoom, J. Mahseredjian, U. Karaagac, Fast investigation of control interaction risks in PV parks using eigenvalue analysis in Modelica, *Electric Power Systems Research*, Vol. 251, 2026,112316.

[9] L. Meng, U. Karaagac, A. Pavani, J. Mahseredjian, and K. Jacobs, "Examination of EMT-Type Impedance Scanning Techniques for Small Signal Stability Assessment of Inverter Based Resources," IEEE Trans. Power Delivery, vol. 40, no. 3, pp. 1607–1620, June 2025.

979-8-3315-8138-1